

# Port Based Modeling of Spatial Visco-Elastic Contacts

Stefano Stramigioli and Vincent Duindam\*

Control Laboratory, Faculty of EEMCS, University of Twente, 7500AE Enschede, The Netherlands

*In this paper, the geometrical description of viscoelastic contacts is described using physical modeling concepts based on energy conservation and network theory. The proposed model is on one side simple enough to be used in real time applications and on the other captures the geometrical features and coupling of a complete spatial geometric unisotropic contact.*

**Keywords:** Contacts; Geometry; Port-Hamiltonian

## 1. Introduction

The model of contacts is of fundamental importance in robotics since most of interesting situations like grasping, walking and mechanical interaction, do feature mechanical contact. The normal component of a contact has been vastly studied and has led to the Kelvin–Voight model and the better Hunt–Crossley model (Hunt and Crossley 1975) which has been analytically studied in Marhefka and Orin (1999). Detailed models concerning tangential friction instead can be found in Armstrong-Hlouvry et al. (1994). An excellent reference on soft finger contacts is Cutkosky and Wright (1986).

The first model to the knowledge of the authors which treats the complete geometry of contacts from a kinematical point of view is Montana (1989a,b). In this model the geometry of rolling is described

using the differential geometric description of the curvature of the contacting surfaces, but no dynamics is treated and the bodies are considered in contact at all times.

A nice analysis on controllability of rolling contacts can be found in Marigo and Bicchi (2000) and for a general review on grasping and contacts the reader is addressed to Bicchi and Kumar (2000).

In this paper, we will show build a geometric port-Hamiltonian model of a contact which is able to describe no-contact to contact transition, rolling and contact viscoelasticity at the same time. The presented model, being lumped, is a big simplification of the continuous mechanic effects of material deformation, but at the same time, due to its geometrical description is very valuable for its light computational load and could be used in real time control.

The paper is organized as follows: in Section 3 the kinematics of three-dimensional (3D) contacts will be quickly reviewed, in Section 4 the major contribution will be presented by first describing the used interconnection structure and then the elastic and viscous description. Section 5 will illustrate some simulation results and Section 6 will draw some conclusions and address possible future research topics.

## 2. Background

In this paper, we use a network modeling approach based on Dirac structures (Courant 1990, van der Schaft and Maschke 1995, van der Schaft et al. 1996,

\*E-mail: V.Duindam@ieee.org

Correspondence to: S. Stramigioli, Control Laboratory, Faculty of EEMCS, University of Twente, 7500AE Enschede, The Netherlands. E-mail: S.Stramigioli@ieee.org

Received 9 January 2004; Accepted 15 October 2004.  
Recommended by A. Astolfi and A.J. Van der Schaft.

Bloch and Crouch 1999, Stramigioli 2001). In this technique the concept of a power port is of fundamental importance. A power port is a pair of dual vectors whose intrinsic dual product is power:

$$(f, e) \in V \times V^*, \quad (1)$$

where  $f$  is called a flow,  $e$  an effort,  $V$  is a vector space and  $e(f) \in \mathcal{R}$  represents the instantaneous power passing through the port. In this paper,  $V$  will have the structure of a Lie algebra since this will allow to rigorously talk about spatial mechanics as shown in the following sections.

Any power continuous interconnection can be expressed using a Dirac structure which can be defined in a complete coordinate free way for finite and infinite dimensional spaces (van der Schaft and Maschke 2002). For the sake of space and conciseness we only say that it is geometrically a subspace of  $V \times V^*$  and as such any finite dimensional Dirac structure where  $V = V_1 \times \dots \times V_n$ , can be represented in Kernel representation by the following equation:

$$Ee + Ff = 0, \quad (2)$$

where  $e \in V, f \in V^*$  and  $E, F$  are in general time varying matrices such that the rank of  $[E \ F]$  should be equal to the dimension of  $V$  and should satisfy the following condition:

$$EF^T + FE^T = 0. \quad (3)$$

This latter condition implies that each element  $(f, e)$  belonging to the Dirac structure, or in other words all the possible  $(f, e)$  which are allowed by the network constraints, are such that  $e(f) = 0$  which is nothing else than Tellegen's theorem (Tellegen 1952). This allows to have a rigorous description of a network structure which can be directly used for analysis.

### 3. Kinematics of Contacts

In Montana (1989a) the kinematics of two contacting bodies is presented. This analysis does not consider the case of non contacting bodies which is important for the detection of collision and does not allow a straight forward coordinate-free interpretation. In Visser et al. (2002) the analysis of Montanais has been extended to non contacting bodies and in Duindam and Stramigioli (2003) a clean coordinate-free formulation has been presented. In this last work, based on the relative configuration  $H_2^1$  of the two bodies, the differential geometric description of their surfaces  $S_1$  and  $S_2$  and their relative twist  $T_2^1 \in \mathfrak{se}(3)$ , the velocity of their minimal distance contact points

$p_1 \in S_1$  and  $p_2 \in S_2$  is calculated providing an implicit formulation of a section of the following form describing the surfaces:

$$\alpha(H_2^1, T_2^1) : S_1 \times S_2 \rightarrow TS_1 \times TS_2. \quad (4)$$

Using the last mapping it is possible to track the motion of the points with minimal distance of the two convex bodies under consideration. We indicate the distance between this two points with  $\Delta$  and we address the reader to Duindam and Stramigioli (2003) for more details.

In Lie group terms, the relative configuration of the two contacting bodies can be studied using  $SE(3)$ . The relative instantaneous motion instead, can be studied using the Lie algebra  $\mathfrak{se}(3)$  associated to  $SE(3)$ . This algebra is 6D and corresponds to the six possible motions of a rigid body.

## 4. Viscoelastic Description

The general scheme which is presented follows the port representation shown in Fig. 1 where it can be seen that a Dirac structure expresses the power continuous interconnection between the contacting bodies, the elastic energy storage of the contact and the (free) energy dissipation part.

### 4.1. The Dirac Structure of the Contact

The purpose of the Dirac structure is to provide the correct, energy consistent relations between the ports that connect the rigid bodies and the storage and dissipation elements. This Dirac structure is not

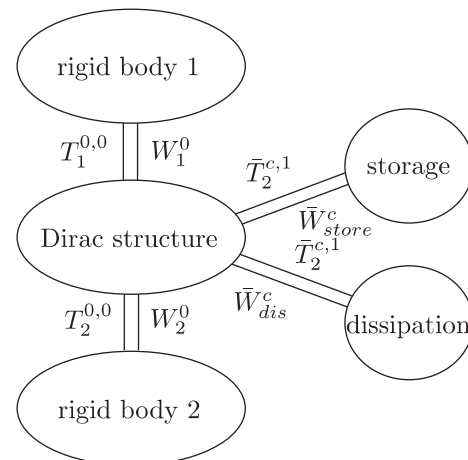


**Fig. 1.** Setup of the model: the contact forces are realized by elastic storage and dissipation, interconnected by a Dirac structure between the two rigid bodies that are in contact.

constant in time, since the connection of the storage and dissipation elements depends on whether there is contact or not. If the bodies are moving freely without touching, there should be no interaction forces from the dissipation and damping elements.

To monitor whether the Dirac structure should switch or not, we use the kinematics equations which are presented in Duindam and Stramigioli (2003). We define the binary signal  $s_\Delta$  as

$$s_\Delta = \begin{cases} 1 & \text{if } \Delta \geq 0, \\ 0 & \text{if } \Delta < 0, \end{cases}$$

so  $s_\Delta = 1$  if there is no contact and  $s_\Delta = 0$  if there is contact. We will use this variable in the equations for the Dirac structure.

We start by constructing the relative velocity of the two bodies, since both the storage and the dissipation depend only on this velocity. So, denoting by  $T_2^{1,1}$  the relative twist of body 2 with respect to body 1, we need as the first part of the Dirac structure (represented in the kernel form  $Ee + Ff = 0$ )

$$E \begin{pmatrix} W_1^0 \\ W_2^0 \\ W_{21}^1 \end{pmatrix} + F \begin{pmatrix} T_1^{0,0} \\ T_2^{0,0} \\ T_2^{1,1} \end{pmatrix} = \begin{pmatrix} 0 \\ 0 \\ 0 \end{pmatrix}, \quad (5)$$

where

$$E := \begin{pmatrix} 0 & 0 & 0 \\ \mathbb{I}_6 & 0 & (s_\Delta - 1)\text{Ad}_{H_0}^T \\ 0 & \mathbb{I}_6 & (1 - s_\Delta)\text{Ad}_{H_0}^T \end{pmatrix} \quad (6)$$

and

$$F := \begin{pmatrix} (1 - s_\Delta)\mathbb{I}_6 & (s_\Delta - 1)\mathbb{I}_6 & \text{Ad}_{H_1}^0 \\ 0 & 0 & 0 \\ 0 & 0 & 0 \end{pmatrix}, \quad (7)$$

where we used the switching element in  $E$  to switch off the contact forces  $W_{21}^1$  when there is no contact. The matrix  $F$  and  $E$  which clearly also satisfy the rank condition, then also contains the switching element in such a way that the power continuity condition  $EF^T + FE^T = 0$  for all values of  $s_\Delta$ .

If we consider a geometric description of the bodies as undeformable for the purpose of modeling, we allow the distance  $\Delta$  between  $p_1$  and  $p_2$  to become negative as shown in Fig. 2. This means that we virtually allow the two bodies  $B_1 \cap B_2 \neq \emptyset$ .

Under the assumptions previously explained of convexness, there are two unique points  $p_1 \in S_1$  and  $p_2 \in S_2$  in the region  $\partial(B_1 \cup B_2)$  (see Fig. 2) whose connecting line  $l_n$  is normal to the surfaces in  $p_1$  and  $p_2$ .

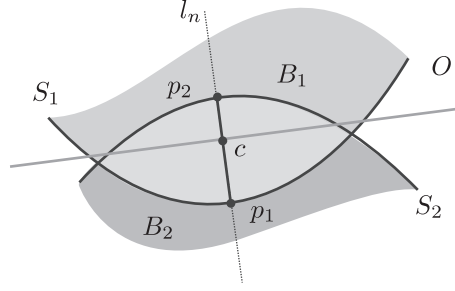


Fig. 2. The geometrical undeformed contact model.

Furthermore, given a point  $c \in l_n$ , there is a unique plane  $O$  orthogonal to  $l_n$  and passing through  $c$ .

We can therefore choose 6 basis vectors (screws) belonging to  $\mathfrak{se}(3)$ . In order to decompose the motion between relative motions involving elastic storage of energy and not, we will choose two screws representing pure distinct rotations around two axis living on  $O$  and passing through  $c(r_x, r_y)$  (which are two screws with zero pitch), and the other basis screws as the rotation around  $l_n(r_z)$  (again a screw with zero pitch), and the three translations  $(t_x, t_y, t_z)$  (which are screws with infinite pitch).

We can now decompose  $\mathfrak{se}(3)$  in the direct sum of two subspaces<sup>1</sup>  $R := \text{span}\{r_x, r_y\}$  and  $\text{span}\{t_x, t_y, r_z, t_z\}$  which turns out to be equal to the Lie algebra  $\mathfrak{se}(2) \times T$  of motions on  $O$  ( $\mathfrak{se}(2)$ ) together with<sup>2</sup> the normal motion along  $l_i(T)$ :

$$\mathfrak{se}(3) = R \oplus (\mathfrak{se}(2) \times T),$$

that is, as the direct sum of two subspaces. We can indicate the projection of a twist  $T_1^2$  defined by this decomposition as

$$P_{R,c} : \mathfrak{se}(3) \rightarrow \mathfrak{se}(2) \times T; \quad T_1^2 \rightarrow PT_1^2. \quad (8)$$

For any linear operator, there is an adjoint operator which maps dual elements corresponding to “wrenches”

$$P_{R,c}^* : \mathfrak{se}^*(2) \times T^* \rightarrow \mathfrak{se}^*(3); \quad W \rightarrow P^*W \quad (9)$$

in such a way that power is conserved:

$$\langle W | PT_1^2 \rangle = \langle P^*W | T_1^2 \rangle.$$

<sup>1</sup>It is important to note that this decomposition is only dependent on the choice of the position of  $c$  and NOT on the choices of  $r_x$  and  $r_y$  as long as they are linear independent and lying on the plane  $O$ .  
<sup>2</sup>Notice that this is not a semi-direct group product, but a normal group product.

We can write this last decomposition/projection part in kernel form (where the projected wrench  $P^*W_{21}^c$  is just the sum of the wrenches from the storage and dissipation elements) to obtain the second part of the Dirac structure:

$$E \begin{pmatrix} W_{21}^1 \\ \bar{W}_{\text{dis}}^c \\ \bar{W}_{\text{store}}^c \end{pmatrix} + F \begin{pmatrix} T_2^{1,1} \\ \bar{T}_{2(\text{dis})}^{c,1} \\ \bar{T}_{2(\text{store})}^{c,1} \end{pmatrix} = \begin{pmatrix} 0 \\ 0 \\ 0 \end{pmatrix}, \quad (10)$$

where

$$E := \begin{pmatrix} 0 & 0 & 0 \\ 0 & 0 & 0 \\ \mathbb{I}_6 & -\text{Ad}_{H_1}^T P^* & -\text{Ad}_{H_1}^T P^* \end{pmatrix} \quad (11)$$

and

$$F := \begin{pmatrix} P\text{Ad}_{H_1^c} & -\mathbb{I}_4 & 0 \\ P\text{Ad}_{H_1^c} & 0 & -\mathbb{I}_4 \\ 0 & 0 & 0 \end{pmatrix}. \quad (12)$$

We can combine both parts and eliminate  $(T_2^{1,1}, W_{21}^1)$  to obtain the complete Dirac structure with ports  $(T_1^{0,0}, W_1^0), (T_2^{0,0}, W_2^0), (\bar{T}_{2(\text{store})}^{c,1}, \bar{W}_{\text{store}}^c)$  and  $(\bar{T}_{2(\text{dis})}^{c,1}, \bar{W}_{\text{dis}}^c)$  as shown in Fig. 1. It is possible to see that the complete Dirac structure is:

$$E \begin{pmatrix} W_1^0 \\ W_2^0 \\ \bar{W}_{\text{store}}^c \\ \bar{W}_{\text{dis}}^c \end{pmatrix} + F \begin{pmatrix} T_1^{0,0} \\ T_2^{0,0} \\ \bar{T}_2^{c,1} \\ \bar{T}_2^{c,1} \end{pmatrix} = 0, \quad (13)$$

where

$$E := \begin{pmatrix} \mathbb{I}_6 & 0 & (s_\Delta - 1)\text{Ad}_{H_0}^T P^* & (s_\Delta - 1)\text{Ad}_{H_0}^T P^* \\ 0 & \mathbb{I}_6 & (1 - s_\Delta)\text{Ad}_{H_0}^T P^* & (1 - s_\Delta)\text{Ad}_{H_0}^T P^* \\ 0 & 0 & 0 & 0 \\ 0 & 0 & 0 & 0 \end{pmatrix} \quad (14)$$

and

$$F := \begin{pmatrix} 0 & 0 & 0 & 0 \\ 0 & 0 & 0 & 0 \\ (s_\Delta - 1)P\text{Ad}_{H_0^c} & (1 - s_\Delta)P\text{Ad}_{H_0^c} & -\mathbb{I}_4 & 0 \\ (s_\Delta - 1)P\text{Ad}_{H_0^c} & (1 - s_\Delta)P\text{Ad}_{H_0^c} & 0 & -\mathbb{I}_4 \end{pmatrix}. \quad (15)$$

## 4.2. The Elastic Coupling Description

The elastic storage element is used to represent the elastic energy that is (reversibly) stored in the compressed surfaces of the bodies that are in contact. As explained earlier, its port is 4D with port variables  $\bar{T}_{2(\text{store})}^{c,1}$  and  $\bar{W}_{\text{store}}^c$ . It is important to understand that this decomposition does NOT exclude any tangential force on the contact, but only excludes pure rolling of the bodies from any energetical influence.

The energy as stored in the element is represented by a function  $V$

$$V : \text{SE}(2) \times T \rightarrow \mathbb{R}; \quad V : \bar{H} \mapsto V(H),$$

where  $\bar{H}$  denotes the element of the group  $\text{SE}(2) \times T$  that describes the deformation (translation in three directions plus rotation around the vertical axis) of the surfaces. Even if other representations are possible, if we represent the twist  $\bar{T}_{2(\text{store})}^{c,1}$  as a 6D twist with the first two elements (rotations in the contact plane) equal to zero, we can compute  $\bar{H}$  just like in the 6D case: by integrating the twist  $\bar{T}_{2(\text{store})}^{c,1}$  as

$$\bar{H}(t) = \int_0^t \tilde{\bar{T}}_{2(\text{store})}^{c,1}(\tau) \bar{H}(\tau) = d\tau.$$

The resulting  $\bar{H}$  will be a  $4 \times 4$  matrix of the form

$$\bar{H} = \begin{pmatrix} \cos(\theta) & -\sin(\theta) & 0 & x \\ \sin(\theta) & \cos(\theta) & 0 & y \\ 0 & 0 & 1 & z \\ 0 & 0 & 0 & 1 \end{pmatrix},$$

where  $\theta$  is the rotation angle around the vertical axis. The function  $V(\bar{H})$  can now be any lower-bounded function (zero for  $\bar{H} = \mathbb{I}_4$ ) to describe the energy associated to a deformation  $\bar{H}$ . The wrench generated at a deformation  $\bar{H}$  is finally equal to

$$W_{\text{store}}^c = \text{Ad}_{\bar{H}}^T dV(\bar{H}).$$

Unfortunately, the partial derivative of  $V$  over  $\bar{H}$  is not so easy to compute since  $\bar{H}$  is globally redundantly represented by a matrix, not a vector due to topological reasons. A simple solution is to take  $\theta, x, y, z$  as representation of the deformation instead, such that the equation becomes

$$\begin{aligned} & (0 \ 0 \ \bar{w}_\theta \ \bar{w}_x \ \bar{w}_y \ \bar{w}_z)^T \\ & = \text{Ad}_{\bar{H}}^T \left( 0 \ 0 \ \frac{\partial V}{\partial \theta} \ \frac{\partial V}{\partial x} \ \frac{\partial V}{\partial y} \ \frac{\partial V}{\partial z} \right)^T. \end{aligned} \quad (16)$$

A different solution that is often presented is to use a two-covariant tensor called the *stiffness tensor*  $K$  to

define the energy function  $V$  implicitly. Around equilibrium,  $K$  is defined such that  $K\delta T$  is the change in spring force, resulting from a small motion in the direction  $\delta T$ . Globally, the stiffness tensor can be defined only using a connection (Howard et al. 1995, Zefran and Kumar 1997). The potential function  $V$  is then constructed from  $K$  at the minimum by integration of the forces (see Stramigioli 2001 for the details).

#### 4.2.1. Handling Anisotropy and Curvature

Using Hertzian theory (Harris 1990), we can study each body elastic properties: we can consider a compression of each of the bodies separately against a flat, infinitely rigid plane. Assuming no tangential load for the moment as it is done in the Hertzian theory, we can consider an elliptical contact patch.<sup>3</sup> This patch will have a shape corresponding to the radius curvature quadric (also called Dupin indicatrix)  $\mathcal{R}(p)$  defined as

$$\mathcal{R}(p) := \{\zeta \in T_p S \text{ s.t. } \langle \zeta, P g_*(p) \zeta \rangle = 1\}, \quad (17)$$

where  $P$  and  $g_*(p)$  are related to the surface description and its curvature in  $p$  as explained in detail in Duindam and Stramigioli (2003).

We assume that the characterization of the elliptic contact patch and its forces are related by three factors:

- The normal compression ( $-\Delta$ ).
- The curvature of the body in the contact point  $p_i$  ( $g_*(p_i)$ ).
- The possible unisotropic properties of the material at the contact point.

If we now consider direct contact and loading of  $B_1$  and  $B_2$  in the points  $p_1$  and  $p_2$ , we assume that an elliptic contact patch will increase around the initial contact points and that this patch lies in the plane  $O$ . The shape of the patch is related to the patches obtained in the contact surface and differential geometrically speaking is directly dependent on the relative curvature of the surfaces in the following way:

$$\mathcal{R}(c) = (\mathcal{R}_1(p_1) + \mathcal{R}_2(p_2)), \quad (18)$$

where  $\mathcal{R}_i$  indicates the radius-curvature of body  $B_i$ .

Clearly, in order to be able to compute Eq. (18) as the sum of two quadrics, we have to consider  $p_1 = p_2$  which can be done considering the initial contacting situation.

In a similar way, due to possible anisotropy of the materials there can be direction dependent stiffnesses in the contact.

In order to take these effect into account, we can associate a stiffness information to each point of the contacting surfaces and then calculate a corresponding geometrical anisotropic stiffness during contact based on them. Once this stiffness is defined, it can be used in the projection plane in order to integrate the projected twists and calculate the corresponding wrenches as explained.

In mathematical terms we can proceed as follows. We can associate to each point of the surfaces a two covariant tensor based on  $\text{se}(2) \times T$  corresponding to a stiffness:

$$K_i : S_i \rightarrow (\text{se}(2) \times T)_2, \quad i = 1, 2. \quad (19)$$

The previous mappings are in differential geometric terms called tensor bundles. By clearly making an approximation, we can then consider both tensors defined in the same point  $c$  considering the initial contact situation as also done to calculate Eq. (18). Under this assumption, it is meaningful to consider

$$K(c) := (K_1^{-1}(p_1) + K_2^{-1}(p_2))^{-1} \quad (20)$$

as a representative stiffness of the contact. To understand this, it is sufficient to realize that in case one of the two contacting materials is much softer than the other, the resulting combined stiffness  $K(c)$  is almost equal to the one with the smallest stiffness.

*4.2.1.1. The choice of the point.*  $c \in l_n$ . It is now possible to find a physical way to uniquely identify the position of  $c \in l_n$  (see Fig. 2) in order to decompose motions based on the elastic properties of the material. In order to give a mathematical expression we first need to define a projection operator which gives the normal component of the stiffness tensor:

$$P_n := (\text{se}(2) \times T)_2 \rightarrow \mathfrak{R}; \quad K \mapsto K(\hat{T}, \hat{T}), \quad (21)$$

where  $\hat{T}$  indicates a unit vector in the direction of  $l_n$ . Using this operator, we can then uniquely define the position of  $c$  as:

$$c := (1 - \alpha)p_1 + \alpha p_2 \quad \text{where } \alpha := \frac{P_n(K_1(p_1))}{P_n(K(c))}. \quad (22)$$

The intuition of Eq. (22) is easily explained: suppose that  $B_2$  is much harder than  $B_1$ . This implies that  $P_n(K_2)$  will be much bigger than  $P_n(K_1)$ . This implies that  $P_n(K) \simeq P_n(K_1)$  and therefore  $\alpha \simeq 1$ . This means

<sup>3</sup>This can be considered correct in a first approximation, but more general consideration can be made. Due to the complexity of more involved patches shapes, they will not be considered in this paper.

that  $c$  will be very close to  $p_2$  which makes a lot of sense since  $B_2$ , being much harder, will deform the least.

*4.2.1.2. Anisotropy.* A crucial point at this stage is that the elastic anisotropy of the material can be handled as a metrical property and coordinate deformations can be applied in such a way that the contact would be described in new coordinates for which the materials would have relative unity uniform stiffness. Clearly, this change of coordinates does have effect on the contact patch shape which would change accordingly. In geometrical terms, the new principal directions of the relative contact patch can be calculated by looking at the eigen vectors of the original undeformed patch quadric  $\mathcal{R}(c)$  with respect to the relative stiffness metric  $K(c)$ . In this new situation we obtain an equivalent contact with a different rotated contact patch, between two homogeneous materials. Analytically we can proceed as follows. Under the condition that there is no coupling among the normal stiffness, the rotational one and the tangential one, it is possible to find two lines  $l_x, l_y \in \mathcal{O}$  by means of which we can define four screws  $r_n, t_n, t_x, t_y$  which are an orthonormal base of  $\text{se}(2) \times T$  with respect to the metric  $K(c)$ .  $r_n$  is a zero pitch screw along  $l_n$  corresponding to a pure rotation around  $l_n$  and  $t_n, t_x, t_y$  are infinite pitch screws corresponding to translations respectively in the directions  $l_n, l_x$  and  $l_y$ . Using the base  $B_{K(c)} := \{t_x, t_y, t_n, r_n\}$  for  $\text{se}(2) \times T$ , a numerical representation for  $K(c)$  becomes by construction the identity matrix  $I_{4 \times 4}$ .

On the other hand, a numerical representation of  $\mathcal{R}(c)$  using the base elements  $t_x, t_y$  would in general not result in a diagonal matrix which would correspond with the principal curvature directions along the basis vector. For this reason, we can implement a second partial change of coordinates which implements a pure rotation in the plane spanned by  $t_x$  and  $t_y$  in order to have coordinates in which the radius-curvature is oriented with the coordinate axis. Such a map can be implemented by:

$$\bar{R} : \mathbb{R}^4 \rightarrow \mathbb{R}^4 \text{ s.t. } \begin{pmatrix} x \\ y \\ z \\ \theta \end{pmatrix} \mapsto \begin{pmatrix} R & 0 & 0 \\ 0 & 1 & 0 \\ 0 & 0 & 1 \end{pmatrix} \begin{pmatrix} x \\ y \\ z \\ \theta \end{pmatrix},$$

where  $R$  is an orthonormal matrix which has as rows the normalized eigenvectors of  $\mathcal{R}(c)$  calculated with respect to the metric  $K(c)$ . In this way, we can define for the compliant contact an energy function

$$\bar{V} : \mathbb{R}^4 \rightarrow \mathbb{R}, \quad (23)$$

which abstracts from the compliant properties of the materials of the two bodies and which has the relative radius-curvature aligned with the first two coordinates. The total normalizing change of coordinates is therefore

$$N(c) : \text{se}(2) \times T \rightarrow \mathbb{R}^4 \text{ s.t. } v \mapsto \bar{R} \cdot (t_x \ t_y \ t_n \ r_n) v, \quad (24)$$

which is a linear map and has as such an adjoint  $N^*$  which maps the corresponding wrenches in the opposite direction:

$$N^*(c) : (\mathbb{R}^4)^* \rightarrow \text{se}^*(2) \times T^* \text{ s.t. } f \mapsto (t_x \ t_y \ t_n \ r_n)^* \bar{R}^T f. \quad (25)$$

The only step left is the definition of an energy function  $\bar{V}$  which can be either quadratic (giving rise to a linear spring) or not.

**Remark 1.** The change of coordinates has used the tensor  $K(c)$  which is representing the stiffness of the material. In general the stiffness is not a tensor, but it can be defined as such when a geometric connection is considered (Howard et al. 1995, Zefran and Kumar 1997). In our case, the natural connection which could be used is the one associated to the exponential coordinates of the Lie group  $\text{SE}(2) \times T$  which being a commutative group gives rise to basis coordinates and therefore a symmetric stiffness. For a non quadratic energy function this would be position dependent and not equal to  $K(c)$ , but for the geometrical considerations we made we consider  $K(c)$  as representative.

*4.2.1.3. The complete picture.* The previous considerations can be applied to any relative contacting situation of the bodies. This implies that at each instant the points  $p_1, p_2$  can be computed integrating the section of Eq. (4) and therefore the line  $l_n$  is consequently defined. Based on  $K_1(p_1)$  and  $K_2(p_2)$  the point  $c$  can be calculated using Eq. (22). Once  $c$  is available, the plane  $\mathcal{O}$  is uniquely determined and therefore it is possible to uniquely project a relative motion belonging to  $\text{se}(3)$  on  $\text{se}(2) \times T$  along  $R$  using the projection operator of Eq. (8). This projection can than be transformed through  $N$  as defined in Eq. (24). The resulting vector can be directly integrated due to the commutativity in the exponential coordinates of  $\text{SE}(2) \times T$ . This results in the elastic state which generates a force which is calculated using  $d\bar{V}(x, y, z, \theta)$ . The corresponding elastic repulsive force is then equal to

$$W = P^* N^* d\bar{V}(x, y, z, \theta), \quad (26)$$

and this completes the elastic model of the contact. In the complete structure presented here,  $N P$  should be substituted in Eq. (13) to  $P$ .

It is important to realize that the elastic function  $\bar{V}$  is left general. This implies that different elastic models can be implemented based on the linear Kelvin–Voight model or the more general non linear Hunt–Crossley model (Hunt and Crossley 1975).

Clearly, when the elastic load reaches a certain threshold, slipping occurs. This will be briefly handled in Section 4.4.

### 4.3. The Viscous Part

The dissipative part can be handled in a similar way to the elastic one. As we did for the elastic part, using the tensor fields reported in Eq. (19) we can define damping fields for the surfaces

$$B_i : S_i \rightarrow (\text{se}(2) \times T)_2, \quad i = 1, 2. \quad (27)$$

The resulting field which will characterize the damping will be resultant of a series interconnection (in the network sense) of the two elements which similarly to Eq. (20) can be calculated as

$$B(c) := (B_1^{-1}(p_1) + B_2^{-1}(p_2))^{-1}. \quad (28)$$

This can be directly used as a linear dissipation following the line of the Kelvin–Voigt model by considering the linear map corresponding to the previous quadratic form which is a map like:

$$B^{\sharp}(c) : \text{se}(2) \times T \rightarrow \text{se}^*(2) \times T^* \quad (29)$$

or this information can be used to create a geometrical extension of the Hunt–Crossley model (Hunt and Crossley 1975) by considering for example:

$$B_H^n(c) : \text{se}(2) \times T \rightarrow \text{se}^*(2) \times T^* \\ \text{s.t. } v \mapsto B^{\sharp}(c)N^{-1}(c) \begin{pmatrix} x^n & 0 & 0 & 0 \\ 0 & y^n & 0 & 0 \\ 0 & 0 & z^n & 0 \\ 0 & 0 & 0 & \theta^n \end{pmatrix} N(c)v, \quad (30)$$

where  $(x, y, z, \theta)$  is the state of the elastic energy  $\bar{V}$  as introduced in Eq. (23).

### 4.4. Slipping

A lot of research is going on in the geometrical modeling of slipping by the authors and a detailed description will be reported in a forthcoming paper. In this section, we briefly give the basic ideas on how

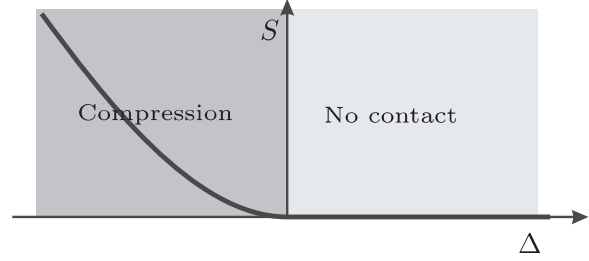


Fig. 3. The threshold function for slip detection.

slipping can be handled within the presented framework because we believe this is useful for completeness. From a microscopical point of view, slip occurs when the elastic coupling between the two bodies reaches a threshold of extension. In such a situation the elastic bindings break and relative motion occurs. When motion occurs, the elastic extension up to the moment of slip is retained and will play a role during the stick phase. A simplified efficient model of the slip effect can be obtained from a microscopical point of view defining the following two functions:

$$V_{\text{slip}} : \text{se}(2) \rightarrow \mathfrak{R} \quad (31)$$

and

$$S : T \rightarrow \mathfrak{R}. \quad (32)$$

The first function  $V_{\text{slip}}$  associates to a tangential elastic load an energy value. This function could be also strictly related to the elastic energy function  $\bar{V}$ , but not necessarily.

The threshold function  $S$  associates instead to the current compression  $\Delta \in T$  a maximum energetical value after which slip occurs. This function will clearly be strictly decreasing and have a shape similar to the one reported in Fig. 3. An analytical expression of  $S$  and  $V_{\text{slip}}$  based on physical principles will be presented in future work. Slip is then detected when the following condition is satisfied:

$$V_{\text{slip}}(h) > S(\Delta), \quad (33)$$

where  $(h, \Delta) \in \text{se}(2) \times T$  indicates the geometrical state of the elastic spring.

## 5. Simulations

We implemented the 3D kinematics and dynamics model in the simulation package 20sim (<http://www.20sim.com>), and simulated the dynamics of two ellipsoids bouncing on each other and on the floor under the influence of gravity. Since there are three

objects, we need to have three copies of the contact model (one between each pair of objects) to be able to model all contact situations. Figure 4 shows a 2D schematic setup of the model. The sub-models are implemented using screw bond graphs (Paynter 1960,

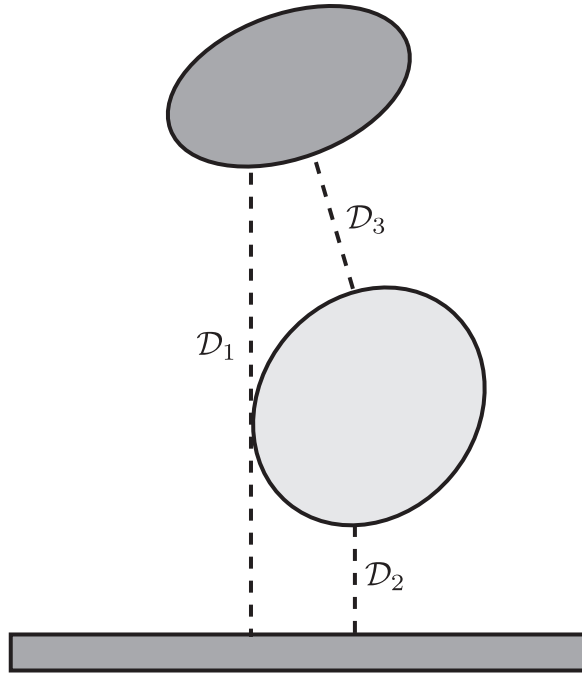


**Fig. 4.** Schematic setup of the simulation model. We use three copies of the contact model to model all possible collisions between the three objects.

Stramigioli 2001), which allow for easy modeling of the power ports to capture the energy balance of the system. We use relatively soft settings for the spring to be able to see more clearly what happens.

We drop the two ellipsoids at some distance right above each other, with zero initial velocity. Figures 5 and 6 show the results, indicating also the following time instants in the simulation:

- (a) The two objects start from a certain height, with some distance between them, the largest distance is between the black ellipsoid and the ground.
- (b) The grey ellipsoid hits the ground first and compresses a bit. When the black ellipsoid hits the grey, the grey is penetrated more into the ground.
- (c) The two ellipsoids start to roll over each other.
- (d) As the black ellipsoid rolls over the grey, it approaches the ground fast.
- (e) The black ellipsoid touches the ground.
- (f) Both ellipsoids roll away, creating a distance between them.

## 6. Conclusion and Future Work

This paper has presented a geometrical, energetically consistent model of the contact dynamics between two convex bodies whose surface viscoelastic properties are described by two, possibly anisotropic, tensor fields defined on the surfaces. The model is able to handle a lot of linear and non-linear models and can

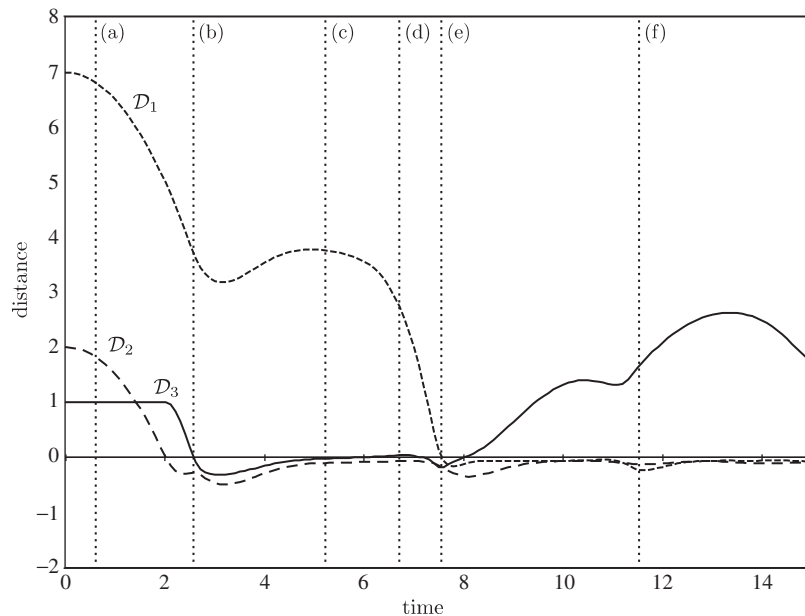


**Fig. 5.** Time evolution of the distances between the three objects. The labels  $D_1$ ,  $D_2$ ,  $D_3$  correspond to the labels in Fig. 4, and the labels (a)–(f) correspond to the labels in Fig. 6.

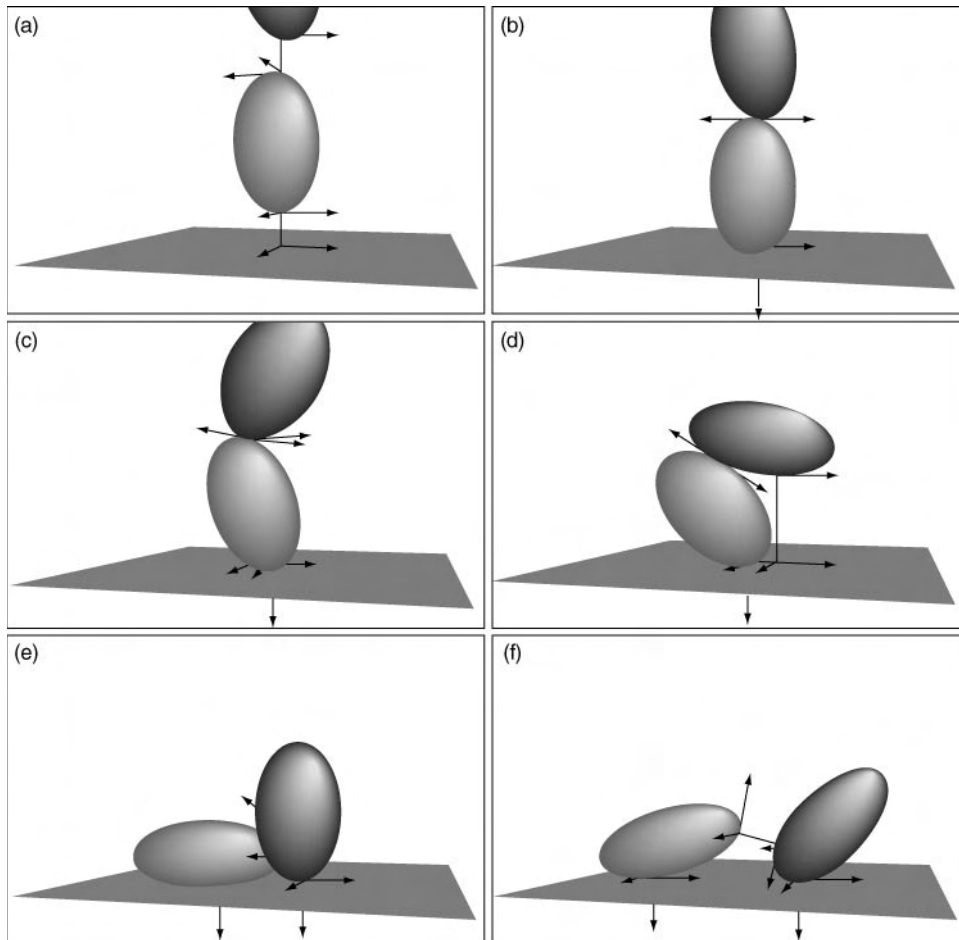


**Fig. 6.** Snapshots of the simulation of two ellipsoids bouncing on each other and on the floor. The labels (a)–(f) correspond to the labels in Fig. 5. The plots also show the contact frames, attached to the generalized contact points at each object.

be the basis for a more physical description of the contact dynamics.

Slipping has been only introduced and a future paper will report a detailed analysis on how to handle slip and stick in this framework.

A future and important extension to this work would clearly be an identification and validation stage which would prove the validity of the model in real experiments. This would be of great value since the model is geometrically complete and at the same time computationally not very heavy and this has great advantages for real time applications like the space application RokViss (Landzettel et al. 2002).

## Acknowledgement

This work has been done in the context of the European sponsored project GeoPlex with reference code IST-2001-34166. Further information is available at <http://www.geoplex.cc>

## References

- Bloch AM, Crouch PE. Representation of dirac structures on vector spaces and nonlinear lcv-circuits. In: Proceedings of symposia in pure mathematics, differential geometry and control theory (Hermes H, Ferraya G, Gardner R, Sussman H (eds)) 1999; 64: 103–117
- Armstrong-Hlouvry B, Dupont P, Canudas de Wit C. A survey of models, analysis tools and compensation methods for the control of machines with friction. *Automatica* 1994; 30(7): 1083–1138
- Bicchi A, Kumar V. Robotic grasping and contact: a review. In: Proceedings of the IEEE international conference on robotics and automation, San Francisco, CA, USA, pp 348–353, 2000
- Courant TJ. Dirac manifolds. *Trans Amer Math Soc* 1990; 319: 631–661
- Cutkosky MR, Wright PK. Friction, stability and the design of robotic fingers. *Int J Robot Res* 1986; 5(4): 20–37
- Duindam V, Stramigioli S. Modeling the kinematics and dynamics of compliant contact. In: 2003 IEEE international conference on robotics and automation, Taipei, Taiwan, 2003

- Harris TH. Rolling bearing analysis. 3rd edn. J. Wiley and Sons, 1990
- Howard WS, Zefran M, Kumar V. On the  $6 \times 6$  stiffness matrix for three dimensional motions. In: Proceedings of the 9th world congress of the IFToMM, Italy, 1995
- Hunt KH and Crossley FRE. Coefficient of restitution interpreted as damping in vibroimpact. *ASMEJAM* 1975; 42: 440–445
- Landzettel K, Brunner B, Beyer A, Krmer E, Preusche C, Steinmetz BM, Hirzinger G. Rokviss verification of advanced tele-presence concepts for future space missions. In: Proceedings of 7th ESA workshop on advanced space technologies for robotics and automation 'ASTRA 2002', Noordwijk, The Netherlands 2002
- Marhefka DW, Orin DE. A compliant contact model with nonlinear damping for simulation of robotic systems. *IEEE Trans Syst, Man, Cybernet – Part A: Syst Humans* 1999; 29(6): 566–572
- Marigo A, Bicchi A. Rolling bodies with regular surface: controllability theory and applications. *Trans IEEE Autom Control* 2000; 45(9): 1586–1599.
- Montana David J. The kinematics of contact and grasp. *Int J Robot Res* 1989a; 7(3): 17–32
- Montana DJ. The kinematics of contact with compliance. In: Proceedings of the IEEE conference on robotics and automation, 1989b, pp 770–774
- Paynter HM. Analysis and design of engineering systems. MIT Press, Cambridge, MA, 1960. Course 2.751
- Stramigioli S. Modeling and IPC control of interactive mechanical systems: a coordinate free approach. LNCIS, Springer Verlag, London, 2001
- Tellegen BDH. A general network theorem, with applications. *Philips Res Rep* 1952; 7: 259–269
- van der Schaft A, Maschke BMJ. The Hamiltonian formulation of energy conserving physical systems with external ports. *Archiv für Elektronik und Übertragungstechnik* 1995; 49(5/6): 362–371
- van der Schaft A, Maschke BMJ. Hamiltonian formulation of distributed-parameter systems with boundary energy flow. *J Geom Phys* 2002; 42: 166–194
- van der Schaft, Arjan, Dalsmo M, Maschke BMJ. Mathematical structures in the network representation of energy-conserving physical systems. In: Proceedings of the 35th conference on decision and control, Kobe, Japan, 1996, pp 201–206
- Visser M, Stramigioli S, Heemskerk C. Screw bondgraph contact dynamics. In: Proceedings of IROS2002, Loussanne, CH, 2002
- Zefran M, Kumar V. Affine connections for the Cartesian stiffness matrix. In: Proceedings of the 1997 IEEE international conference on robotics and automation, Albuquerque, New Mexico, 1997